Applied Catalysis B: Environmental 119–120 (2012) 123–131

Contents lists available at SciVerse ScienceDirect

Applied Catalysis B: Environmental

journal homepage: www.elsevier.com/locate/apcatb

N-doped carbon prepared by pyrolysis of dicyandiamide with various $MeCl_2 \cdot xH_2O$ (Me = Co, Fe, and Ni) composites: Effect of type and amount of metal seed on oxygen reduction reactions

Chang Hyuck Choi [a], Sung Hyeon Park [a], Seong Ihl Woo [a,b,*]

[a] Department of Chemical and Biomolecular Engineering, Korea Advanced Institute of Science and Technology, Daejeon 305-701, Republic of Korea
[b] Graduate Study of EEWS (WCU) and Center for Ultramicrochemical Process, Korea Advanced Institute of Science and Technology, Daejeon 305-701, Republic of Korea

ARTICLE INFO

Article history:
Received 23 December 2011
Received in revised form 13 February 2012
Accepted 28 February 2012
Available online 5 March 2012

Keywords:
Nitrogen doped carbon
Oxygen reduction reaction
Metal seeds
Polymer electrolyte membrane fuel cells

ABSTRACT

N-doped carbon was prepared from dicyandiamide as the source for both carbon and nitrogen. Dicyandiamide was pyrolyzed at 900 °C on various metal chlorides ($MeCl_2 \cdot xH_2O$, Me = Co, Fe, and Ni) to clarify the effects of metal type on the properties of the N-doped carbon. The results showed that electrochemical and physical characteristics of the N-doped carbon were altered by the type of metal seed. The N-doped carbon from Co showed the best performance in oxygen reduction reactions (ORRs) and the order of ORR activity was N-doped carbon from Co > Fe > Ni. Raman and XPS studies revealed that the metal type during pyrolysis step determined degree of sp^2-carbon network, and ORR activity of N-doped carbon was improved as the degree of sp^2-carbon network increased. The effects of the amount of metal precursor on activity of ORRs and rate of H_2O_2 formation were faint but the carbonization yield of dicyandiamide increased as the amount of metal precursor increased. The catalysts optimized by altering the type and amount of metal seed showed a 0.60 V (vs. Ag/AgCl) onset potential and a 42% oxygen reduction reactivity at 0.40 V (vs. Ag/AgCl) compared to that of a commercial Pt/C catalyst.

1. Introduction

In efforts to expand the range of application of heteroatom doped carbon, various methods to dope diverse heteroatoms (e.g. Li, P, B, and N) into carbon or graphite structures and the resultant characteristics of the materials have been extensively reported [1–5]. Nitrogen is considered to be the ideal dopant due to its similar atomic size to carbon [6]. Nitrogen doping into carbon alters structural, mechanical, and electrical properties of carbon. In particular, nitrogen doping causes structural deformation of carbon and it increases the n-type conductivity by acting as an electron donor [7,8]. Doped nitrogen also induces charge delocalization for adjacent carbon atoms due to its strong electron affinity [9,10].

As a new non-metal electro-catalyst of polymer electrolyte membrane fuel cells (PEMFCs), N-doped carbon has attracted attention due to its low price and high activity [9–21]. However, the active site of N-doped carbon towards the ORRs has not yet been clearly identified. Many groups have argued that metal–nitrogen complex, $Me–N_x$ (Me = transition metals), presented in Me-porphyrine or Me-phtalocyanine is an active site for ORRs [22–24], such as the $Co–N_2$ structure proposed by Bashyam and Zelenay [25]. However, it was shown that the $Me–N_x$ structure was destroyed in the catalysts prepared by heat-treatment of metal-macrocycle composites at high temperature, which is required for synthesizing N-doped carbon [26–28]. Furthermore, when metal was removed through acid treatment, the activity towards ORRs was improved [29]. Another proposed active site of N-doped carbon for ORRs is nitrogen adjacent carbon atoms [9]. As noted above, the carbon atoms adjacent to the doped nitrogen atoms show a slightly positive charge due to charge delocalization, and this facilitates the break of oxygen molecules by bonding in the form of parallel diatomic adsorption mode onto the carbon atoms.

Although transition metals such as Co and Fe used for synthesizing N-doped carbon do not act as active sites after pyrolysis, they play important roles in the carbonization of feed chemicals or the doping structure of nitrogen into carbon (e.g. pyridinic-, pyrrolic-, graphitic-nitrogen, and pyridinic-oxide). Nallathambi et al. argued that transition metals facilitated the formation of pyridinic- and graphitic-N sites in the carbon lattice during pyrolysis [29]. Ozaki et al. evaluated N-doped carbon nanoshells synthesized by pyrolysis of Me-phtalocyanine (Me = Co, Fe, and Ni) [30]. From the results, they showed that the characteristics of carbons varied and their activities toward the ORRs were significantly affected by the metal

* Corresponding author at: Department of Chemical and Biomolecular Engineering, Korea Advanced Institute of Science and Technology, 373-1 Gusong-dong, Yuseong-gu, Daejeon 305-701, Republic of Korea. Tel.: +82 42 350 3918; fax: +82 42 350 8890.
E-mail address: siwoo@kaist.ac.kr (S.I. Woo).

0926-3373/$ – see front matter © 2012 Elsevier B.V. All rights reserved.
doi:10.1016/j.apcatb.2012.02.031

type. In addition to the case of pyrolized Me-phthalocyanine, where N-doped carbon was synthesized through various methods such as pyrolysis of Me-porphyrin [31] or Me-triethylenetetramine [32], and a chemical vapor deposition (CVD) method with acetonitrile as carbon and nitrogen sources [33], it was also reported that the ORR activity was changed according to the type of metal used. This shows that even though transition metals cannot participate in the reaction as an active site, they have remarkable effects on the formation of active sites for the ORRs.

Here, we discuss the roles of metal seeds and characteristics of N-doped carbon grown on the seeds. The catalysts were prepared through pyrolysis of dicyandiamide (DCDA) as both carbon and nitrogen sources. DCDA, as a precursor of N-doped carbon, has many merits such as low price and easy handling (solid phase and non-flammability). Three different catalysts were prepared and characterized based on various metal precursors ($MeCl_2 \cdot xH_2O$, Me = Co, Fe, and Ni) to elucidate the effects of metal sources on the synthesis of N-doped carbon. In addition, four different catalysts were prepared by pyrolysis of composites having various ratios of metal precursor ($CoCl_2 \cdot 6H_2O$) to DCDA in order to optimize the activity towards ORRs.

2. Experimental

2.1. Preparation of nitrogen doped carbons from various metal precursors

N-doped carbons were obtained through pyrolysis of homogeneous mixtures of DCDA and metal precursors. In 300 mL of ethanol, 5 g of DCDA (Aldrich, USA) and 1 g of $MeCl_2 \cdot xH_2O$ (Me = Co, Fe, and Ni and x = 6, 4, and 6, respectively; Aldrich, USA) were mixed. After 30 min of stirring to dissolve the chemicals, the solvents were vaporized using an evaporator (BUCHI R-200, Swiss) at 80 °C and 300 mbar. The obtained gel-like products were dried in an oven at 100 °C for 12 h to remove residual ethanol. The powders showed purple, black-brown, and chartreuse colors for the mixtures of DCDA with $CoCl_2$, $FeCl_2$, and $NiCl_2$, respectively. Each powder (5 g) was loaded on a quartz boat and was placed in the middle of a quartz tube reactor 60 cm in length and 10 cm in diameter. Under a 60 cm^3/min Ar flow, the temperature of the reactor was raised at a rate of 10 °C/min. Pyrolysis of the powder was carried out at 900 °C for 3 h. The acquired black powder was stirred in a 400 mL mixture of nitric acid (60 wt.%, Dae Jung, Korea) and hydrochloric acid (35 wt.%, Dae Jung, Korea) aqueous solutions (v:v = 1:3) at room temperature for 12 h to remove metal species in the N-doped carbon products. Finally, the black powder was retrieved through filtering, washing with DI-water, and drying. These catalysts were abbreviated as Me-DCDA-BA or Me-DCDA-AA, where Me indicates the type of metal and, BA and AA denote before acid treatment and after acid treatment, respectively.

To study the effects of the amount of cobalt seed during preparation on the ORR activity, N-doped carbon samples preparing from different amounts of cobalt seed were also prepared. The preparation method was identical to the procedure described above. $CoCl_2 \cdot 6H_2O$ was used as a metal precursor and added quantities were varied from 1 to 3, 5, and 7 g. The samples comprising residues after acid treatment were gathered and were denoted as Co-DCDA-AA-X according to the amount of $CoCl_2 \cdot 6H_2O$ added (X indicates the amount of $CoCl_2 \cdot 6H_2O$ added; X = 1, 3, 5, and 7).

2.2. Characterizations

Physical characterizations of the catalysts were performed by thermogravimetry analysis (TGA), X-ray diffraction (XRD), transmission electron microscopy (TEM), X-ray photoelectron spectroscopy (XPS), element analysis (EA), Raman spectroscopy, and Brunauer–Emmett–Teller (BET) surface area analysis. The experimental details are as follows. TGA data was gathered with a TG209F3 at a 10 °C/min heating rate under an air atmosphere. XRD patterns were acquired from a D/MAX-2500 (Rigaku) operated at 40 kV and 100 mA. Step-scan patterns were collected in the 20–80° (2-theta ranges) range with 0.01° step size and 1°/min scan speed. TEM images were taken with a JEM2100-F (JEOL Ltd.) operated at 200 kV. XPS spectra were obtained with Mg Kα as an X-ray source and 8.4 kV to 14 mA operating power. Surface compositions of the catalysts from the XPS peaks were calculated by using sensitivity factors of 0.296 and 0.477 for carbon and nitrogen, respectively. An EA was carried out to obtain the bulk compositions of the catalysts using a FlashEA 1112. Doping concentration of the nitrogen in the carbon was expressed by the atomic ratio of nitrogen atoms to carbon atoms measured by EA or XPS. The data from Raman spectroscopy were obtained by a LabRAM HR UV/Vis/NIR with a 514 nm Ar ion CW laser source. A BET surface area analysis was performed on a Micrometrics ASAP 2010 apparatus at 77 K. Before measurement, all samples were degassed and dehydrated at 200 °C for 2 h.

Electrochemical properties were examined using a three-electrode-type beaker cell equipped with a Pt wire counter electrode (ALS Co., 002233), an Ag/AgCl reference electrode (ALS Co., 012167), and a rotating ring disk electrode (ALS Co., 011162), using an electrochemical analyzer (CH Instruments, Inc., CHI700D) and a rotator (ALS Co., RRDE-3A). The working electrodes were prepared by the thin-film electrode method. The catalysts (10 mg) were dispersed in an ink solution (1 mL; DI-water (15), 5 wt.% Nafion in water (4), isopropyl alcohol (1); the number in parentheses indicates the volumetric ratio) followed by sonication, and then catalyst inks (5 μL) were dropped onto glassy carbon of a rotating ring disk electrode. The catalyst inks were dried at room temperature. 20 cycles of cyclic voltammetry (CV) experiments were conducted in deaerated 1 M $HClO_4$ electrolyte for activation of the catalysts with a 15 mV/s scan rate from −0.22 to 0.578 V (vs. Ag/AgCl). Data from the last cycle was selected for characterization. The ORR experiments were conducted in O_2 saturated 1 M $HClO_4$ electrolyte with a 5 mV/s scan rate and 2000 rpm rotating velocity from 0.82 to −0.08 V. For comparison of ORR activity, commercially obtained Pt/C (30 wt.%, E-tek) was also examined at same conditions. H_2O_2 formation yield was derived from the current at Pt ring disk electrode. Constant potential (1.2 V) was applied on Pt ring disk electrode during ORR experiment. The following equation was used for the calculation of H_2O_2 formation yield:

$$H_2O_2(\%) = 200 \times \frac{I_R/N}{I_R/N + I_D}$$

where I_R and I_D are ring and disk currents, and N is collection efficiency (0.37).

3. Results and discussion

3.1. Effects of metal types for N-doped carbon

3.1.1. Calculated yield of carbon from TGA data

Table 1 presents the non-metal/metal weight ratio of the catalysts before and after acid treatment obtained from TGA results. Here, the amount of metal is obtained by residual mass after TGA experiments, and for the non-metal, which refers to the sum of masses of N-doped carbon components (e.g. C, N, O, or H) excluding metal elements, is calculated from the mass loss during TGA experiment. After acid treatment, a large amount of metal was dissolved from the catalysts. Not all metals, however, were eliminated, even after several iterations of acid treatment as shown in Fig. 1.

Table 1
Measured amounts of non-metal/metal components for Me-DCDA catalysts (Me = Co, Fe, and Ni) before and after acid treatment obtained from TGA results under an air atmosphere.

Composition	Before acid treatment (wt.%)		After acid treatment (wt.%)	
	Non-metal	Metal	Non-metal	Metal
Co-DCDA	60	40	92	8
Fe-DCDA	33	67	81	19
Ni-DCDA	66	34	86	14

The amounts of the precursors and the products were weighed at every step of the experiment. These measurement results and the results obtained from TGA were employed to calculate the yields of the catalysts. It was assumed that all non-metal components were comprised of carbon, and yields were defined as the ratios of amount of the carbon obtained from the product to that of the carbon in DCDA. The yields of the Me-DCDA catalysts are found to be 24.3, 17.0, and 33.2% for Co-DCDA, Fe-DCDA, and Ni-DCDA, respectively. Co, Fe, and Ni are well-known catalysts for carbonization [34–36], and have been applied to the synthesis of many carbon nano-structures such as carbon nano-tubes (CNTs). In the present case, they also showed good carbonization abilities, and Ni in particular showed the best yield for carbon growth.

3.1.2. X-ray diffraction results of the catalysts

Fig. 2 shows the XRD patterns of the obtained catalysts after acid treatment. In Fig. 2, the graphite peaks are denoted as *G*(0 0 0) depending on their crystal planes, and circles, squares, and triangles denote the XRD peaks of metallic Co, Fe, and Ni, respectively. Regardless of the type of metal, the catalysts show a clear (0 0 2) peak of graphite in the XRD results. This indicates that carbon atoms from DCDA are carbonized in the form of graphite through pyrolysis of the mixture of transition metal chloride and DCDA. Metal residues after acid treatment are shown as metallic crystal structures of Co, Fe, and Ni in the XRD results. Iron carbide is formed as a by-product in the case of Fe-DCDA-AA (the peaks have low intensity in the XRD data of the Fe-DCDA and they were not assigned), but no by-products such as oxide or carbide are formed in Co-DCDA-AA or Ni-DCDA-AA.

3.1.3. Morphological analysis from TEM images

Fig. 3 shows TEM images of the catalysts before and after acid treatment. Regardless of the type of metal, all catalysts exist as a mixture of CNT or carbon nano-fiber (CNF) with various radii, lengths, and structures including some bulky carbon masses. Especially in the case of Fe-DCDA (Fig. 3(c) and (d)), most carbon products have CNT with a thin and regular structure, unlike when Co or Ni seeds are used. Comparison between before and after acid treatment (Fig. 3(a)-(b), (c)-(d), and (e)-(f)) clearly indicates that large amounts of metal particles are removed. Open edge sites or hollow carbon spheres are formed in Me-DCDA-AAs through metal dissolution.

The existence of some metal residues is identified even after acid treatment as illustrated in the enlarged in right-hand corner of Fig. 3(b), (d), and (f). As shown in the illustrations, residual metal nano-particles are encapsulated by carbon. Shielding agents obstructing metal dissolution are carbon layers that are deposited on the metal surface. As the carbon layers block the reaction between protons and metal nanoparticles, some metal nanoparticles remain in the catalysts after acid treatment. Especially in the case of Fe-DCDA-AA, large amounts of the residual metal particles are presented as compared to the other catalysts (residual metal amount: Fe > Ni > Co from Table 1) due to the formation of iron carbide, which is not dissolved by acid.

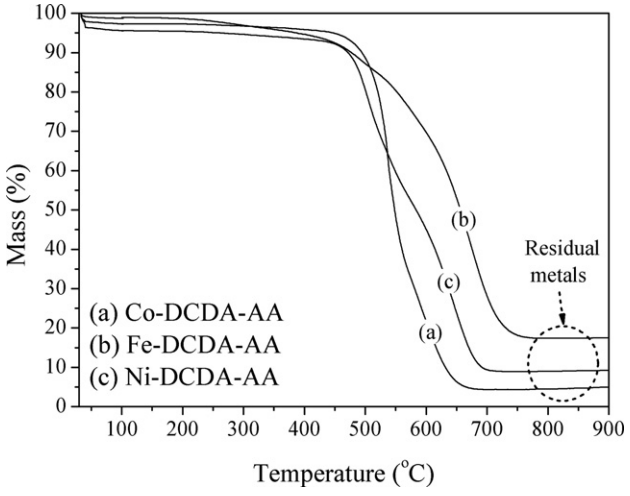

Fig. 1. TGA results of the Me-DCDA-AA (Me = Co, Fe and Ni). A dotted circle indicates the amount of residual metal after several iterations of acid treatment.

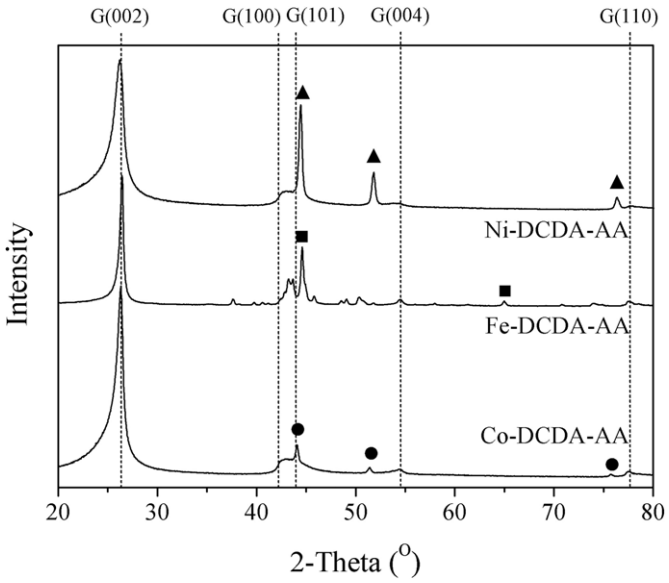

Fig. 2. XRD patterns of the Me-DCDA-AA (Me = Co, Fe and Ni). *G*(0 0 0)s are assigned to the graphite peaks and the peaks of Co, Fe, and Ni are denoted as circles, squares and triangles, respectively.

3.1.4. Analysis of nitrogen doping structures and amounts in Me-DCDA

Fig. 4 shows the results of XPS-N_{1s} for Me-DCDA-AA (Me = Co, Fe, and Ni). Nitrogen takes various forms in the carbon structure and subsequently has a distinct binding energy. In general, nitrogen is doped into the graphite structure in the form of pyridinic-N (398.6 eV), pyrrolic- or graphitic-N (400–402 eV), and pyridinic oxide (402–404 eV) [37]. The assignment of their respective peaks is indicated by dotted lines in Fig. 4 ((a) pyridinic-N, (b) pyrrolic- or graphitic-N, and (c) pyridinic oxide); here, the peaks at each binding energy are deconvoluted with 2.3 of FWHM and 30% of Lorentzian–Gaussian function to optimize the peak assignment. The yields for different doping patterns are summarized in Table 2. All of the catalysts obtained from three different metals show doping patterns of 37.9–44.7% for pyridinic-N, 44.7–47.5% for pyrrolic- or graphitic-N, and 10.0–14.6% for pyridinic oxide. No significant difference in the doping patterns is observed according to the metal type. Doping concentration, however, differs depending on the used metal type. The highest value is found from

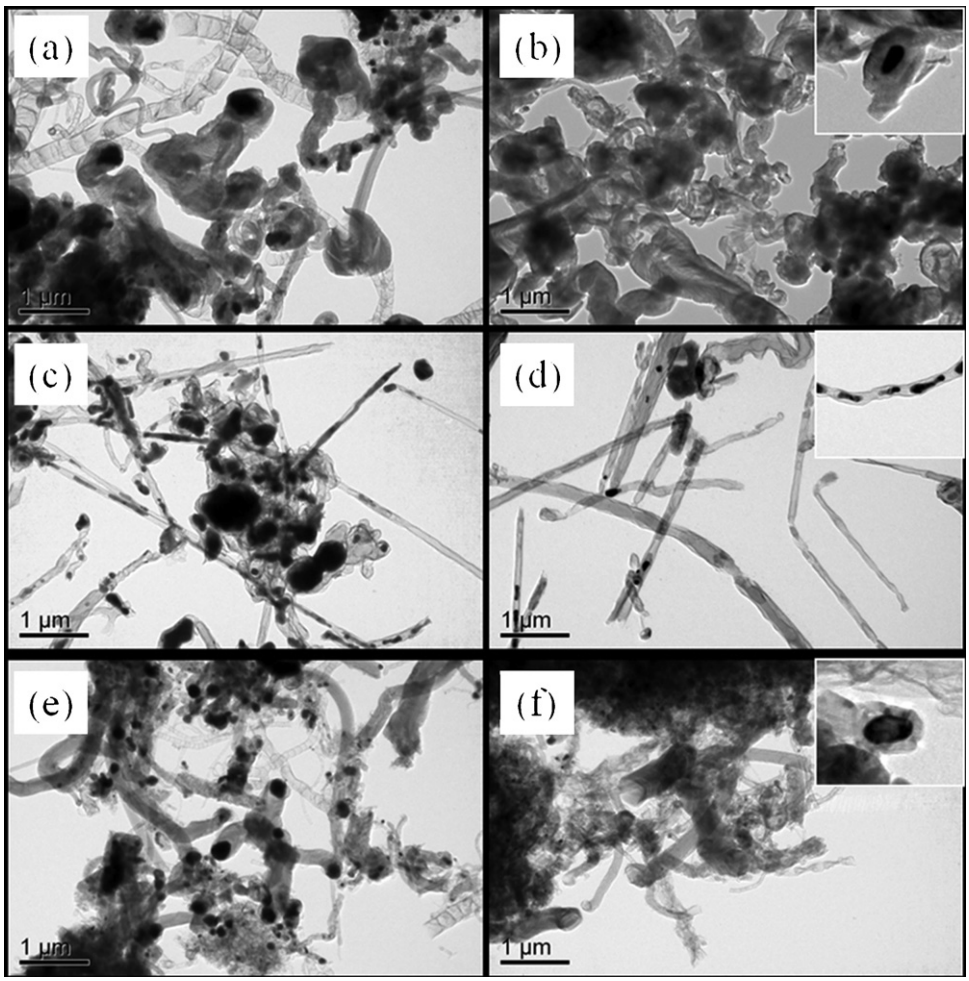

Fig. 3. TEM images of the obtained catalysts before and after acid treatment. TEM images of the Me-DCDA-BAs for Co, Fe, and Ni are shown in (a), (c), and (e) and those of Me-DCDA-AAs for Co, Fe, and Ni are indicated as (b), (d), and (f). The illustrations in the TEM images of Me-DCDA-AAs are magnified figures of residual metals after acid treatment.

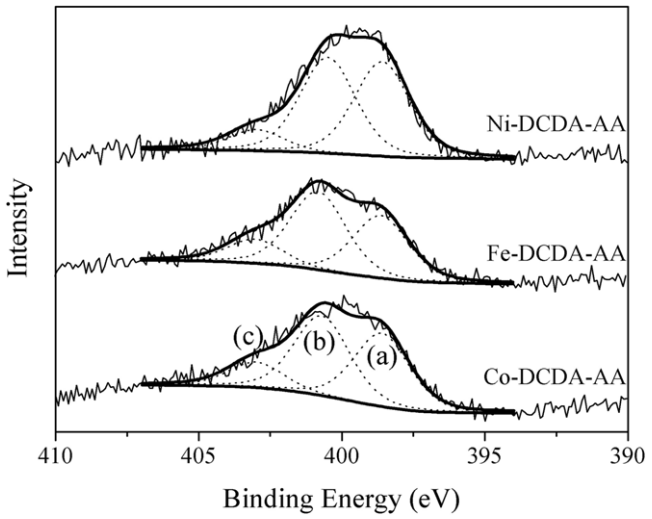

Fig. 4. XPS-N_{1s} data of the Me-DCDA-AA (Me = Co, Fe, and Ni). Peaks are assigned to (a) pyridinic-N, (b) pyrrolic- or graphitic-N, and (c) pyridinic oxide.

Ni-DCDA-AA (3.4) while Co-DCDA-AA (2.5) and Fe-DCDA-AA (2.6) show similar values. In other words, Ni is a very efficient seed metal for nitrogen doping into the carbon compared to Co and Fe.

Table 2
Calculated distribution ratio of nitrogen and doping concentration through peak assignments of XPS results.

Catalysts	Co-DCDA-AA	Fe-DCDA-AA	Ni-DCDA-AA
N/C[a]	2.5	2.6	3.4
N-type (%)			
Pyridinic-	41.0	37.9	44.7
Pyrrolic- or graphitic-	44.7	47.5	45.3
Pyridinic oxide-	14.3	14.6	10.0

[a] ×100, atomic ratio.

Table 3
Bulk compositions and calculated doping concentrations of the prepared catalysts obtained from EA.

Catalysts	C (wt.%)	N (wt.%)	H (wt.%)	Total (wt.%)	N/C[a]
Co-DCDA-AA	86.7	2.6	0.4	89.7	2.9
Fe-DCDA-AA	79.2	1.8	0.3	81.3	1.9
Ni-DCDA-AA	79.6	3.4	0.3	83.3	3.7

[a] ×100, atomic ratio.

The bulk composition of the catalysts through an EA also reveals that N-doping is the most favorable on the Ni seed (Table 3). N-doping concentration calculated through EA is 3.7 for Ni-DCDA-AA, followed by 2.9 for Co-DCDA-AA and 1.9 for Fe-DCDA-AA. The total weight of the EA results does not reach 100%, as oxygen and metals comprising the catalysts are not covered by the EA.

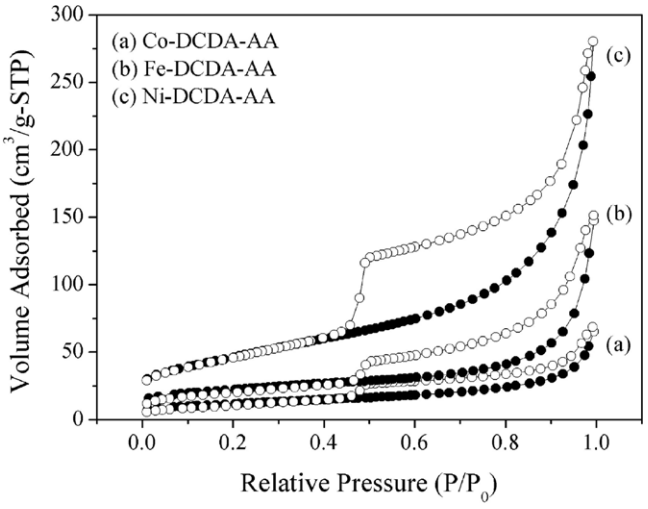

Fig. 5. Adsorption isotherm of Me-DCDA-AA for BET area. Filled circles indicate adsorption and empty circles means desorption onto the surface of (a) Co-DCDA-AA, (b) Fe-DCDA-AA, and (c) Ni-DCDA-AA.

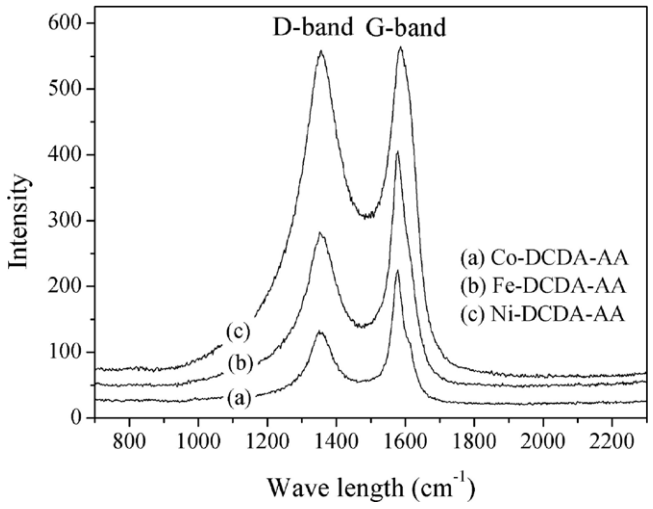

Fig. 6. Raman spectroscopy analysis of (a) Co-DCDA-AA, (b) Fe-DCDA-AA, and (c) Ni-DCDA-AA.

3.1.5. BET area and Raman spectroscopy of the Me-DCDA-AAs

Adsorption isotherms were examined to determine the surface area of the obtained catalysts (Fig. 5). As shown in Fig. 5, all the catalysts show hysteresis due to their unique pore structure. The shapes of the adsorption isotherms arise from the adsorbent having slit-like pores [38]. Carbon has a structure that is constructed with many piled-up graphene sheets, and thus shows this phenomenon.

The BET areas measured from the adsorption isotherms are 42, 78, and 167 m^2/g for Co-, Fe-, and Ni-DCDA-AA, respectively. Tested for comparison, Vulcan carbon XC-72R and multi-walled carbon nano-tubes (MWCNTs) show BET areas of 307.6 and 225.4 m^2/g, respectively. Even though Me-DCDA-AAs include residual metals, these values for Me-DCDA-AAs are much lower than those of Vulcan carbon and MWCNTs, respectively. Calculated with the mass ratio of metal and carbon within the catalysts, the carbon normalized BET areas also show lower values than other carbons. This means that Me-DCDA-AAs have a very small number of pores; this can account for the carbon layer acting as a barrier to proton-penetration.

In Raman spectroscopy of all sp^2-carbon, two conspicuous peaks emerged, at around 1580 cm^{-1} of the G-band and 1352 cm^{-1} of the D-band. The G-band arises from the E_{2g} vibrational mode in the D^4_{6h} symmetry group of graphite crystal planes and is seen for all sp^2-carbon [39]. The D-band originates from lattice distortion in sp^2-hybridized carbon. The D-band is basically a Raman-inactive mode (A_{1g}) but it becomes active due to a reduction of symmetry at or near crystalline edges. However, the D-band behavior is still unclear and it is known that its intensity is affected by the presence of various defects (vacancy, topological defects, impurities, etc.) [40]. Fig. 6 illustrates the results of Raman spectroscopy for Me-DCDA-AAs. The peaks of D- and G-bands are found at wavelengths (cm^{-1}) of (1351, 1577), (1354, 1578), and (1354, 1584) for Co-, Fe-, and Ni-DCDA-AA, respectively. As the amount of nitrogen doping increases, the wavelengths of the D- and G-bands are up-shifted. Bulusheva et al. reported that up-shifting of the D-band could be attributed to new types of disorder in N-doped carbon compared to pure graphite [40]. They showed that up-shift increases as N-doping increases and argued that new types of disorder were induced from N-doping. In addition, the shift of the G-band with increased N-doping is not related to the structural defects, and it is attributed to modification of the electronic structure of graphite.

The ratio of D- and G-band intensities (I_D/I_G) is generally used as a measure of carbon disorder. In the case of the catalysts, Co-, Fe-, and Ni-DCDA-AA present the values of 0.56, 0.66, and 0.99 in I_D/I_G, respectively. The correlation between N-doping concentration and I_D/I_G is shown in Fig. 7. Doping concentration increases as the metal type changes to Co, Fe, and Ni, and this corresponds to the catalysts' tendency of disorder. The results showing that the value of I_D/I_G increases with the N-doping concentration are also supported by the finding of other groups [40,41]. In other words, it can be concluded that not only the amount of nitrogen doping but also the structure and disorder of graphite vary considerably by the type of metal used in N-doped carbon synthesis.

The XPS-C_{1s} analysis also supports that sp^2-bonding in the carbon structure is reinforced when Co is used for carbonization of DCDA. In Fig. 8, the peak at 284.5 eV indicates C—C bonding arisen from sp^2-bonding between carbon atoms. The intensities of the peaks decrease as the seed metal alters from Co and Fe to Ni, meaning that sp^2-bonding structure in the carbon decreases as the tendency. This corresponds to the results from Raman spectroscopy, and it represents that Co is the most effective metal for constructing ordered carbon structure among Co, Fe and Ni.

3.1.6. Electrochemical properties of the catalysts

Fig. 9 shows comparative results of CVs (A) among Me-DCDA-AAs and those of individual catalysts before and after acid-treatment for (B) Co-, (C) Fe-, and (D) Ni-DCDA. As shown in Fig. 9(A), the CV data do not present unique peaks and are similar to the CV results of graphite [42]. The area of the CVs is closely

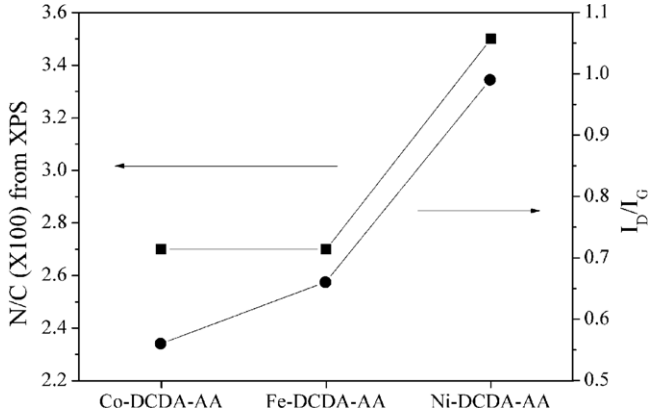

Fig. 7. Correlation between I_D/I_G and N-doping concentration. Squares and circles indicate the N-doping concentration estimated from XPS and the values of I_D/I_G from raman spectroscopy, respectively.

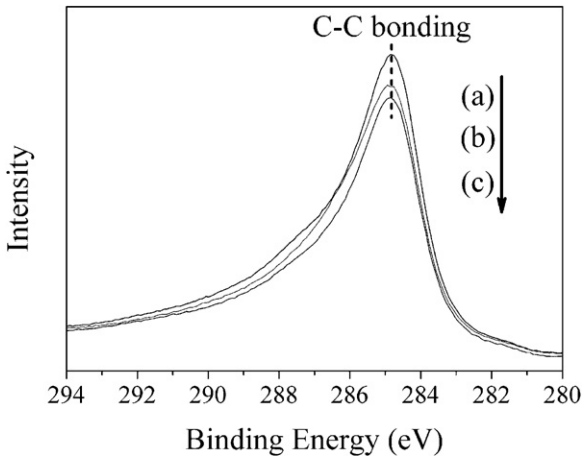

Fig. 8. XPS-C_{1s} results of (a) Co-DCDA-AA, (b) Fe-DCDA-AA, and (c) Ni-DCDA-AA. Dotted line at 284.5 eV indicates C—C bonding of the catalysts.

related with the capacitance of a given material [43]. In Fig. 9(A), the area of CVs decreases in the order of Co- > Fe- ≈ Ni-DCDA-AA and, accordingly, this indicates that the capacitance of Co-DCDA-AAs is the best among the Me-DCDA-AAs.

Catalysts before acid treatment (Me-DCDA-BAs) have unique CV shapes depending on the used metal type (in Fig. 9(B)–(D)). After dissolution of exposed metal particles through acid treatment, however, the catalysts show similar CV shapes and large increment in CV areas compared to before acid treatment; this indicates that the capacitance of the catalysts is improved. This is because the content of N-doped carbon by unit mass increases (Table 1), and greater areas of the carbon surface covered by metal particles become exposed. In other words, this shows that the capacitance of the Me-DCDA catalysts is caused not by metals but by N-doped carbon. Co-DCDA-AA demonstrates the largest capacitance in Fig. 9(A), as it produces the smallest amount of metal residues after acid treatment (from TGA results) and thereby has the highest content of N-doped carbon by unit mass.

The performance of the catalysts towards ORRs was evaluated in oxygen saturated 1 M $HClO_4$ (Fig. 10(A)). ORRs in Co- and Fe-DCDA-AA are initiated at around 0.59 V and 0.62 V (vs. Ag/AgCl), respectively; however, in the case of Ni-DCDA-AA, the reaction originates at much lower voltage than the others, i.e. about 0.45 V (vs. Ag/AgCl). This indicates that the onset potential of ORRs is greatly affected by the type of metal. Limiting current densities of Co- and Fe-DCDA-AA show different values, as it is a function of oxygen diffusion coefficient which is determined by the morphology of the catalysts. Different metal seeds produced various N-doped carbons having different morphology as shown in Fig. 3. Therefore, oxygen diffusion efficiency is also affected by the type of seed metal and results in different limiting current density for Co- and Fe-DCDA-AA. Performance-wise, Co- and Fe-DCDA-AA show similar ORR activities while Ni-DCDA-AA has very low current.

The reactivity of Co-, Fe-, and Ni-DCDA to ORRs before and after metal dissolution is illustrated in Fig. 10(B), (C), and (D), respectively. Regardless of the metal type, the starting voltage of ORRs is up-shifted after acid treatment, and their activities also increase tremendously. This phenomenon is remarkable especially for Co- and Fe-DCDA. This means that N-doped carbon, not a metal, serves as the active site of ORRs. Similar conclusions have been supported by the results of many other researchers [9,14,29].

Not only the ORR activity, but the type of used seed metal also effects ORR reaction pathways: the 2-electron pathway to H_2O_2 formation and the 4-electron pathway to H_2O formation. The amount of H_2O_2 formation during the ORRs is shown in Fig. 11. The results indicate that H_2O_2 formation yield in the reaction is varied by used seed metal type. Co-DCDA-AA produces 22.6% of H_2O_2 at 0.5 V (vs. Ag/AgCl), but Fe-DCDA-AA produces 10.3% of H_2O_2 which is lower than half of the H_2O_2-yield from Co-DCDA-AA.

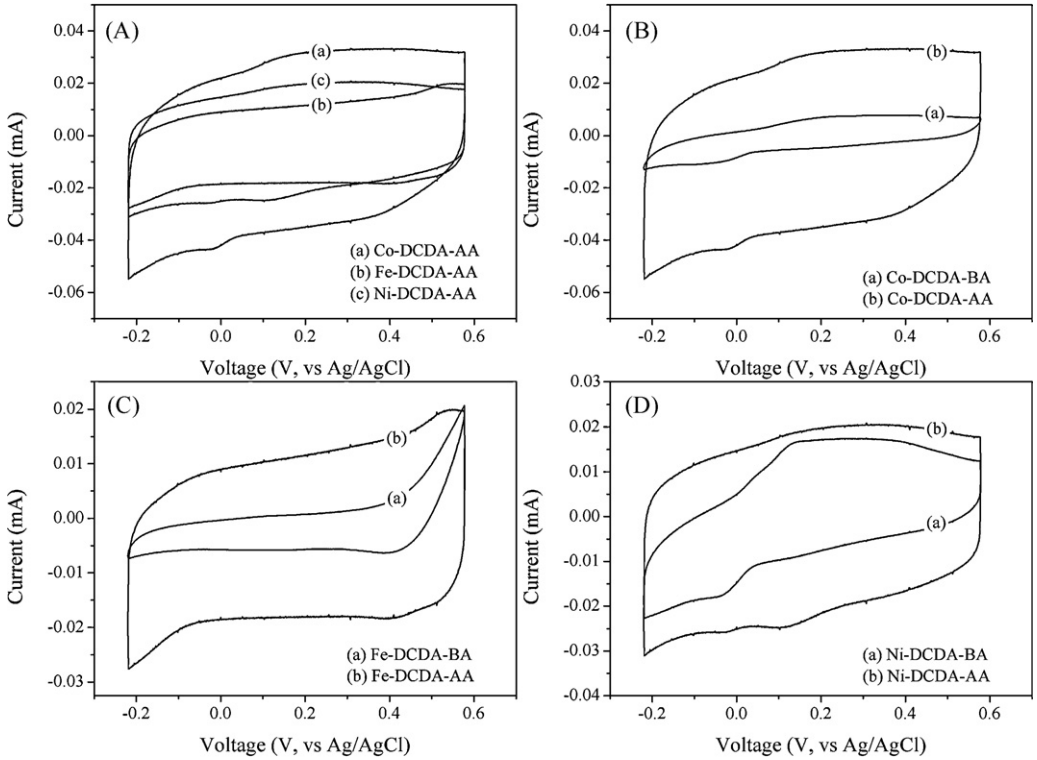

Fig. 9. The results of CVs in deaerated 1 M $HClO_4$. Details of CVs are represented as (A) comparison of Me-DCDA-AAs and difference before and after acid-treatment of (B) Co-, (C) Fe-, and (D) Ni-DCDA.

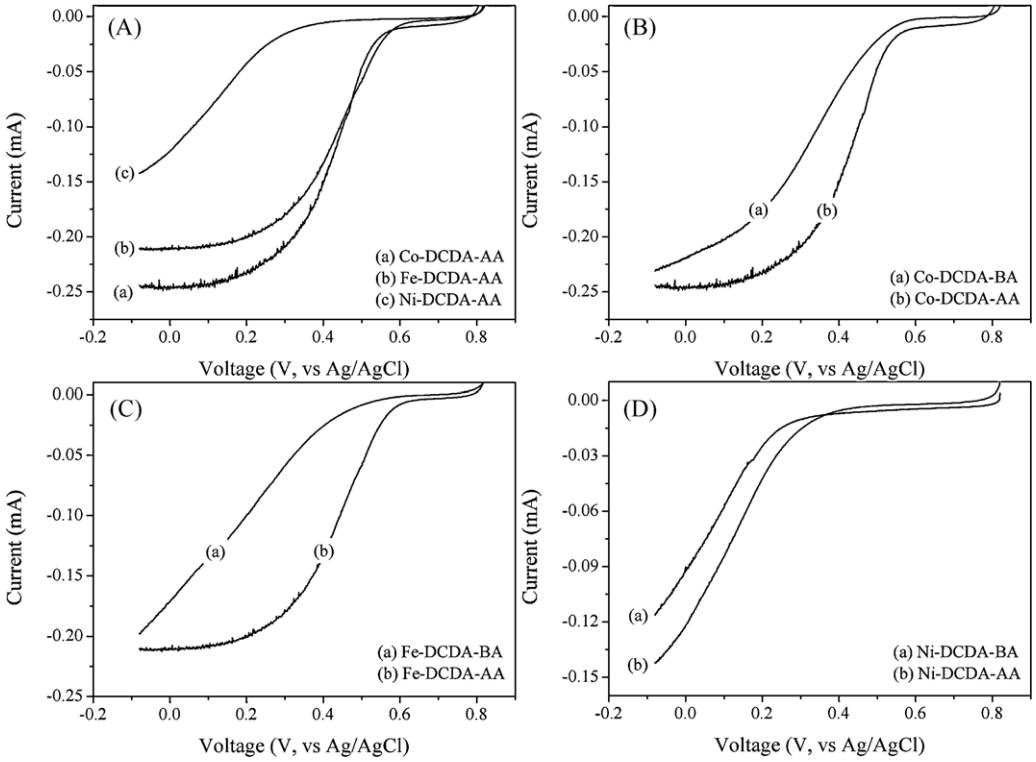

Fig. 10. The results of ORRs in oxygen saturated 1 M $HClO_4$. Details of ORRs are represented as (A) comparison of Me-DCDA-AAs and difference before and after acid-treatment of (B) Co-, (C) Fe-, and (D) Ni-DCDA.

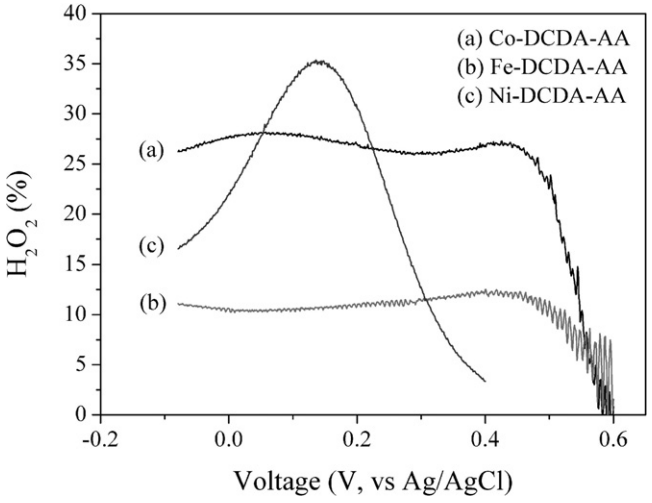

Fig. 11. H_2O_2 production yields of the prepared catalysts during ORRs.

The catalyst with the highest ORR activity is Co-DCDA-AA, and the order of activity is Co-, Fe-, and Ni-DCDA-AA. Several theoretical studies revealed that N-doping in carbon creates active sites towards ORRs [9,11,44]; therefore, increment of N-doping may increase the number of active sites and the ORR activity. However, in this case, N-doping concentrations of the prepared catalysts (Ni- > Fe- > Co-DCDA-AA, from Table 2) do not correspond with the order of ORR activity. Similar results were already reported that the amount of N-doping was not a crucial factor determining ORR activity [17].

Niwa et al. reported that ORR activity of N-doped carbon was improved with increasing sp^2-carbon network [45]. In the case of Me-DCDA-AAs, I_D/I_G values from Raman spectroscopy and intensities of C—C bonding from XPS-C_{1s} show that sp^2-bonding structure in carbon is improved in the order of Ni-, Fe-, and Co-DCDA-AA, and it corresponds well with the order of ORR activity for the catalysts. Large amounts of defects inducing disorder of carbon structure cause intensive breakdown and result in many problems such as increased resistance [41]. In other words, sp^2-carbon structure increases electron transfer rate and improves ORR activity by transferring electrons easily to oxygen molecules. Therefore, it can be concluded that the type of metal alters the degree of sp^2-bonding in carbon structure during carbonization of precursor on it, and it affects ORR activity of the N-doped carbon.

3.2. Effects of metal amount for N-doped carbon

3.2.1. Calculated yield of carbon from TGA data

Table 4 presents the non-metal/metal weight ratio of the catalysts, synthesized with various amounts of metal precursor (X g of $CoCl_2{\cdot}6H_2O$ and 5 g of DCDA, X = 1, 3, 5, and 7 g), based on TGA results. Before acid-treatment, the content of metal (Co) in the catalysts (Co-DCDA-BA-Xs) increases from 40 to 67 wt.% and that of non-metal (N-doped carbon) in the catalysts decreases from 60 to 33 wt.% as the amount of Co precursor is increased. However, all catalysts demonstrate similar composition ratios (i.e. about 90–92 wt.% of N-doped carbon and 8–10 wt.% of Co) after acid treatment (Co-DCDA-AA-Xs) regardless of the amount of $CoCl_2{\cdot}6H_2O$ in the precursor mixture.

The yields of carbon calculated from TGA results and the mass of the products are provided in Fig. 12. As shown in Fig. 12, yields of carbon in Co-DCDA-AA-Xs are 24.3, 57.2, 56.8, and 66.3% for X = 1, 3, 5, and 7, respectively. As the amount of metal precursor is increased, the yield of synthesized carbon also increases and, in particular, it increases exponentially when the weight ratio of $CoCl_2{\cdot}6H_2O$ to DCDA increases from 0.2 (X = 1) to 0.6 (X = 3). From the results, it can be concluded that metal serves as catalysts for carbonization of DCDA and that the yields of carbon do not increase significantly when the ratio of $CoCl_2{\cdot}6H_2O$ to DCDA exceeds 0.6.

Table 4
Measured amounts of metal components for Co-DCDA-*X* catalysts (*X* = 1, 3, 5 and 7) before and after acid treatment through TGA experiments under an air atmosphere.

Amounts of $CoCl_2 \cdot 6H_2O$ (*X* g)	Before acid treatment (wt.%)		After acid treatment (wt.%)	
	Non-metal	Metal	Non-metal	Metal
1	60	40	92	8
3	50	50	91	9
5	38	62	91	9
7	33	67	90	10

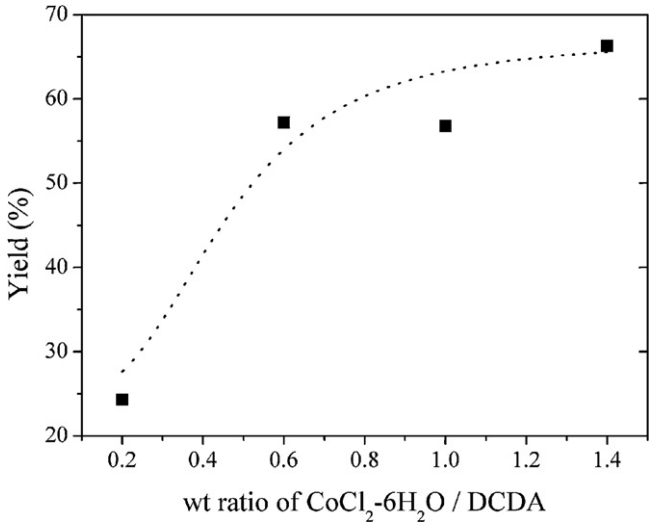

Fig. 12. Calculated yields of carbon for Co-DCDA-AA-*X* catalysts (*X* = 1, 3, 5, and 7) from TGA results and weight of the products.

3.2.2. Electrochemical properties of the catalysts

Fig. 13(A) presents the CV results of Co-DCDA-AA-*X*s in deaerated 1 M $HClO_4$. As expressed with arrows, the areas of CV increase slightly as the amount of Co precursor increases. This increase in area, however, is only minimal, and all catalysts demonstrate similar shapes and properties regardless of the amount of $CoCl_2 \cdot 6H_2O$.

ORR results of the catalysts obtained in oxygen saturated 1 M $HClO_4$ are shown in Fig. 13(B). Regardless of the amount of Co precursors, all the catalysts have similar ORR starting voltages at around 0.60 V (vs. Ag/AgCl), proving that the amount of metals in the precursor mixture is independent of the onset potential. However, the amount of $CoCl_2 \cdot 6H_2O$ in the precursor mixture affects the limiting currents of the catalysts. In this case, Co exposed at the surface of the catalysts was eliminated through acid treatment. Residual Co cannot affect ORR itself because residual Co is covered by several carbon layers (Fig. 3). Moreover, the amount of residual Co is similar regardless of the amount of Co precursor added in the preparation step (Table 4). Therefore, ORR properties, including limiting current, do not have important relationship with the amount of Co precursor itself. However, because Co precursor acted as a seed for carbonization of DCDA and large amount of Co was removed by acid treatment, remaining with newly exposed carbon surface, different amounts of Co precursor could result in different physical properties of N-doped carbon (e.g. morphology, pore size, etc.) during carbon-growth and acid treatment steps. The physical properties determine the oxygen diffusion efficiencies; therefore,

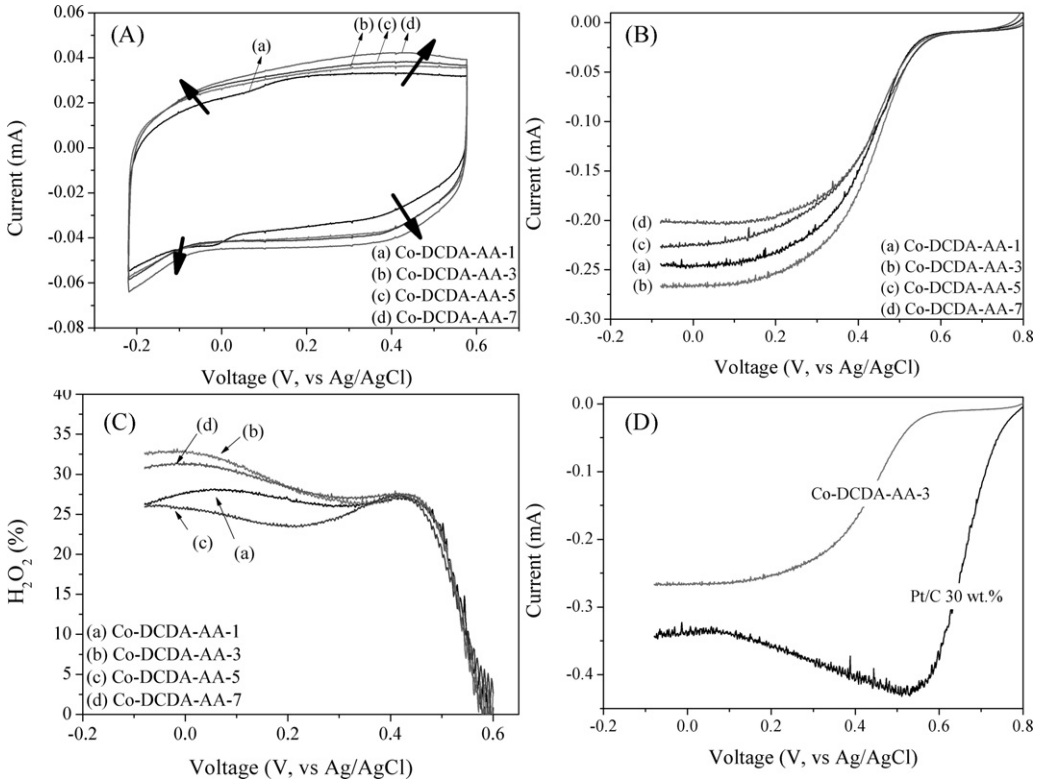

Fig. 13. Electrochemical properties depending on the amounts of $CoCl_2 \cdot 6H_2O$ in precursor mixtures. (A) CVs in deaerated 1 M $HClO_4$, (B) ORRs in O_2 saturated 1 M $HClO_4$, and (C) H_2O_2 production yields during ORRs were examined. (D) ORR activity of the optimized catalyst, Co-DCDA-AA-3, was compared with that of commercial Pt/C.

different limiting currents might be due to different physical properties of N-doped carbon which are affected by the amount of Co precursor.

The catalyst showing the greatest performance is Co-DCDA-AA-3, with the performance decreasing in the order of $X = 1$, 5, and 7 in Co-DCDA-AA-*X*s. All the catalysts have similar H_2O_2 production yields during ORRs, 22.6% at 0.5 V (vs. Ag/AgCl), as shown in Fig. 13(C). It means that the amount of Co does not severely affect the ORR pathway of the catalysts. Co-DCDA-AA-3, an optimized catalyst obtained by altering the type and amount of metal precursors, and a commercial Pt/C catalyst are compared in Fig. 13(D). Co-DCDA-AA-3 demonstrates roughly 0.20 V lower onset potential and 42% that of ORR activity at 0.4 V (vs. Ag/AgCl) compared to Pt/C.

4. Conclusions

N-doped carbons synthesized from pyrolysis of DCDA with various metal types ($MeCl_2 \cdot xH_2O$, Me = Co, Fe and Ni) and amounts were characterized to clarify the effects of seed metal on the catalysts used for oxygen reduction reactions. From the results, it showed that properties of N-doped carbon including physical and electrochemical characteristics are varied by used seed metal type and amount. It is revealed that degree of sp^2-carbon structure is affected by the type of seed metal (Co > Fe > Ni), and it determines ORR activity of N-doped carbon. N-doped carbon from Co exhibited the highest ORR activity, which had the highest degree of sp^2-carbon network among various metal types. The type of seed metal also altered the amount of N-doping in carbon, which induced formation of active sites toward ORRs, however, it did not affect the ORR activity of the N-doped carbon. The amount of metal seed does not change the electrochemical properties significantly including capacitance, ORR activity, and H_2O_2 production yield, but it was related with the yield of carbonization of DCDA during the pyrolysis. The optimized catalyst controlled by the type and amount of seed metal was N-doped carbon based on Co seed metal with 0.6 of metal–DCDA ratio, and it showed 0.60 V (vs. Ag/AgCl) onset potential and 42% oxygen reduction reactivity at 0.4 V (vs. Ag/AgCl) compared to that of a commercial Pt/C catalyst.

Acknowledgement

This work was supported by the National Research Foundation of Korea (NRF) grant funded by the Korea Government (MEST) (No. 2010-0028718).

References

[1] J. Lin, P. Chen, X. Wu, K.L. Tan, Science 285 (1999) 91–93.
[2] T.C.M. Chung, Y. Jeong, Q. Chen, A. Kleinhammes, Y. Wu, Journal of the American Chemical Society 130 (2008) 6668.
[3] R. Mokaya, Y.D. Xia, G.S. Walker, D.M. Grant, Journal of the American Chemical Society 131 (2009) 16493–16499.
[4] L. Novotny, I.O. Maciel, N. Anderson, M.A. Pimenta, A. Hartschuh, H.H. Qian, M. Terrones, H. Terrones, J. Campos-Delgado, A.M. Rao, A. Jorio, Nature Materials 7 (2008) 878–883.
[5] S. Lim, S.H. Yoon, I. Mochida, D.H. Jung, Langmuir 25 (2009) 8268–8273.
[6] A.V. Okotrub, L.G. Bulusheva, A.G. Kudashov, V.V. Belavin, D.V. Vyalikh, S.L. Molodtsov, Applied Physics A: Materials Science and Processing 94 (2009) 437–443.
[7] M. Hayashi, C.L. Sun, H.W. Wang, L.C. Chen, K.H. Chen, Journal of the American Chemical Society 128 (2006) 8368–8369.
[8] M. Terrones, P.M. Ajayan, F. Banhart, X. Blase, D.L. Carroll, J.C. Charlier, R. Czerw, B. Foley, N. Grobert, R. Kamalakaran, P. Kohler-Redlich, M. Ruhle, T. Seeger, H. Terrones, Applied Physics A: Materials Science and Processing 74 (2002) 355–361.
[9] L.M. Dai, K.P. Gong, F. Du, Z.H. Xia, M. Durstock, Science 323 (2009) 760–764.
[10] X.L. Feng, R.L. Liu, D.Q. Wu, K. Mullen, Angewandte Chemie-International Edition 49 (2010) 2565–2569.
[11] A.B. Anderson, R.A. Sidik, N.P. Subramanian, S.P. Kumaraguru, B.N. Popov, Journal of Physical Chemistry B 110 (2006) 1787–1793.
[12] N.P. Subramanian, X.G. Li, V. Nallathambi, S.P. Kumaraguru, H. Colon-Mercado, G. Wu, J.W. Lee, B.N. Popov, Journal of Power Sources 188 (2009) 38–44.
[13] J.R. Dahn, G.C.K. Liu, Applied Catalysis A: General 347 (2008) 43–49.
[14] K.R. Lee, K.U. Lee, J.W. Lee, B.T. Ahn, S.I. Woo, Electrochemistry Communications 12 (2010) 1052–1055.
[15] C.H. Choi, S.H. Park, S.I. Woo, Green Chemistry 13 (2011) 406–412.
[16] C.H. Choi, S.Y. Lee, S.H. Park, S.I. Woo, Applied Catalysis B: Environmental 103 (2011) 362–368.
[17] F. Jaouen, J. Herranz, M. Lefevre, J.P. Dodelet, U.I. Kramm, I. Herrmann, P. Bogdanoff, J. Maruyama, T. Nagaoka, A. Garsuch, J.R. Dahn, T. Olson, S. Pylypenko, P. Atanassov, E.A. Ustinov, ACS Applied Materials and Interfaces 1 (2009) 1623–1639.
[18] G. Liu, X.G. Li, J.W. Lee, B.N. Popov, Catalysis Science and Technology 1 (2011) 207–217.
[19] P. Zelenay, G. Wu, K.L. More, C.M. Johnston, Science 332 (2011) 443–447.
[20] H. Kim, H.S. Oh, J.G. Oh, B. Roh, I. Hwang, Electrochemistry Communications 13 (2011) 879–881.
[21] H. Kim, H.S. Oh, J.G. Oh, W.H. Lee, H.J. Kim, International Journal of Hydrogen Energy 36 (2011) 8181–8186.
[22] B. Wang, Journal of Power Sources 152 (2005) 1–15.
[23] D. Villers, X. Jacques-Bedard, J.P. Dodelet, Journal of the Electrochemical Society 151 (2004) A1507–A1515.
[24] J.P. Dodelet, C. Medard, M. Lefevre, F. Jaouen, G. Lindbergh, Electrochimica Acta 51 (2006) 3202–3213.
[25] P. Zelenay, R. Bashyam, Nature 443 (2006) 63–66.
[26] E. Yeager, Electrochimica Acta 29 (1984) 1527–1537.
[27] K. Wiesener, Electrochimica Acta 31 (1986) 1073–1078.
[28] V.S. Bagotzky, M.R. Tarasevich, K.A. Radyushkina, O.A. Levina, S.I. Andrusyova, Journal of Power Sources 2 (1978) 233–240.
[29] V. Nallathambi, J.W. Lee, S.P. Kumaraguru, G. Wu, B.N. Popov, Journal of Power Sources 183 (2008) 34–42.
[30] J. Ozaki, S. Tanifuji, A. Furuichi, K. Yabutsuka, Electrochimica Acta 55 (2010) 1864–1871.
[31] P. Atanassov, S. Pylypenko, S. Mukherjee, T.S. Olson, Electrochimica Acta 53 (2008) 7875–7883.
[32] Q.Z. Jiang, H.J. Zhang, L.L. Sun, X.X. Yuan, Z.P. Shao, Z.F. Ma, International Journal of Hydrogen Energy 35 (2010) 8295–8302.
[33] R. Côté, G. Lalande, G. Faubert, D. Guay, J.P. Dodelet, G. Dénès, Journal of New Materials for Electrochemical Systems 1 (1998) 7–16.
[34] E. Terrado, M. Redrado, E. Muñoz, W.K. Maser, A.M. Benito, M.T. Martínez, Materials Science and Engineering C 26 (2006) 1185–1188.
[35] L. Durrer, T. Helbling, C. Zenger, A. Jungen, C. Stampfer, C. Hierold, Sensors and Actuators B: Chemical 132 (2008) 485–490.
[36] E. Salernitano, T.D. Makris, L. Giorgi, R. Giorgi, N. Lisi, Diamond and Related Materials 14 (2005) 815–819.
[37] U.S. Ozkan, P.H. Matter, L. Zhang, Journal of Catalysis 239 (2006) 83–96.
[38] J.B. Condon (Ed.), Surface Area and Porosity Determinations by Physisorption, first ed., Elsevier, 2006.
[39] Y. Wang, D.C. Alsmeyer, R.L. Mccreery, Chemistry of Materials 2 (1990) 557–563.
[40] L.G. Bulusheva, A.V. Okotrub, I.A. Kinloch, I.P. Asanov, A.G. Kurenya, A.G. Kudashov, X. Chen, H. Song, Physica Status Solidi B: Basic Solid State Physics 245 (2008) 1971–1974.
[41] O.Y. Podyacheva, Z.R. Ismagilov, A.E. Shalagina, A.V. Ischenko, L.S. Kibis, A.I. Boronin, Y.A. Chesalov, D.I. Kochubey, A.I. Romanenko, O.B. Anikeeva, T.I. Buryakov, E.N. Tkachev, Carbon 47 (2009) 1922–1929.
[42] Z.F. Ren, J.H. Chen, W.Z. Li, D.Z. Wang, S.X. Yang, J.G. Wen, Carbon 40 (2002) 1193–1197.
[43] K.J. Stevenson, J.D. Wiggins-Camacho, Journal of Physical Chemistry C 113 (2009) 19082–19090.
[44] T. Ikeda, M. Boero, S.F. Huang, K. Terakura, M. Oshima, J. Ozaki, Journal of Physical Chemistry C 112 (2008) 14706–14709.
[45] M. Oshima, H. Niwa, M. Kobayashi, K. Horiba, Y. Harada, K. Terakura, T. Ikeda, Y. Koshigoe, J. Ozaki, S. Miyata, S. Ueda, Y. Yamashita, H. Yoshikawa, K. Kobayashi, Journal of Power Sources 196 (2011) 1006–1011.